Supplementary Materials for

Extracellular vesicle formation mediated by local phosphatidylserine exposure drives efficient cell extrusion

Akihito Kira[1], Ichiko Tatsutomi[1†], Keisuke Saito[1†], Machiko Murata[1†], Izumi Hattori[1], Haruna Kajita[1], Naoko Muraki[1], Yukako Oda[2], Saya Satoh[3], Yuta Tsukamoto[3], Seisuke Kimura[4,5], Hiroki Kato[3], Tsuyoshi Hirashima[6,7*], and Kohki Kawane[1*]

*Correspondence: hirashima.tsuyoshi.2m@kyoto-u.ac.jp (T.H.), kawane@cc.kyoto-su.ac.jp (K.K.)

This includes:

Other Supplementary Materials for this manuscript include the following:

Materials and Methods

Plasmid

pCAG-mGFP (palmitoylated EGFP) and pEGFP-actin were purchased from Addgene (14757) and Clontech, respectively. pCAG-EcadSal:GFP was gifted by Dr. A. Nagafuchi. pCAG-MFG-E8 (D89E):GFP and pCAG-Lifeact:mRuby were constructed. Briefly, the MFG-E8 coding sequence amplified from pEF1-MFG-E8 (D89E) (gifted by Dr. S. Nagata (Hanayama et al., 2002)) with the primers 5-ATGCAGGTCTCCCGTGTGCTG-3′ and 5-ACAGCCCAGCAGCTCCAGGC-3′ was subcloned into EcoRI sites in pCAG-mLSR:cGFP (gifted by Dr. M. Furuse (Masuda et al., 2011)). The Lifeact:mRuby coding sequence amplified from Lifeact:mRuby (Addgene, 54674) with the primers 5-GCGGCCGCGCTAGCGCCACCATGGGCGT-3′ and 5-GGTACCTTACTTGTACAGCTGCTCCA-3′ was subcloned into the NheI and KpnI sites in pCAG-mRFP.

Cell culture

MDCKI, MDCKII, and EpH4 cells (gifted from Dr. E. Reichmann) were grown in Dulbecco's modified Eagle's medium (D-MEM) (High Glucose) with L-Glutamine, Phenol Red and Sodium Pyruvate (Wako, 043-30085) including antibiotics (Penicillin-Streptomycin Mixed Solution, Nakarai Tesque, 26253-84) and Fetal Bovine Serum (FBS, HyClone) (5% for MDCKII and 10% for MDCKI and EpH4 cells) (hereinafter referred to as standard culture medium). For the transient gene knockdown experiments, siRNA for each specific gene (Santa Cruz, sc-154404 for *Ano6/TMEM16F*; sc-141186 for *Arf1*; sc-43620 for *Arf6*; sc-41629 for *PC-Pld1*; sc-155377 for

Xkr8; and sc-37007 for the control) were transfected using Lipofectamine™ RNAiMAX Transfection Reagent (Thermo Fisher) into EpH4 cells, together with BLOCK-iT™ Alexa Fluor™ Red Fluorescent Control (Thermo Fisher, 14750100) to monitor siRNA-incorporated cells. Briefly, the transfection reagent and siRNA prepared following the manufacturer's instructions were added to a tissue culture-treated glass-bottom dish (CELLVIEW™ CELL CULTURE DISH, Greiner Bio-One, 627870), and then cells were seeded onto them. Two days after transfection, time-lapse imaging with a laser confocal microscope (TCS SP8, Leica) was performed.

For the transient expression of MFG-E8 (D89E), MDCKII and EpH4 cells with 30–60% confluence on a tissue culture-treated glass-bottom dish were transfected with pCAG-MFG-E8 (D89E) using Lipofectamine™ LTX reagent (Thermo Fisher). Briefly, the standard culture medium was replaced with DMEM, high glucose, no glutamine, no calcium (Thermo Fisher, 21068028) without FBS 30 min before transfection. Transfection was performed according to the manufacturer's instructions, except for the use of DMEM, high glucose, no glutamine, and no calcium also in the step of the plasmid-Lipofectamine complex formation. The medium was changed to the standard culture medium 5 h after transfection. Two days post-transfection, imaging experiments were performed.

To establish a stable transformant expressing membrane-bound GFP, RFP, Actin:GFP, or Lifeact:mRuby, transfection was similarly performed as abovementioned in a 6 cm diameter cell culture dish (VIOLAMO) and 2 d after, the standard culture medium was replaced with the one containing 400 μg/mL G418 sulfate (Wako) or 200 μg/mL HygromycinB (Wako) and cells were cultivated for 10–14 days. Surviving colonies were selected and diluted to obtain single cell-derived clones.

For UV-induced cell extrusion, MDCKII and EpH4 cells were grown to a confluent state on a tissue culture-treated glass-bottom dish. The standard culture medium was replaced with a minimum volume of PBS, and the cells were irradiated using a UV Stratalinker 2400 (Stratagene), followed by time-lapse imaging analysis after further incubation in the standard culture medium for the times indicated in the figure legends.

For mosaic analysis, palmitoylated GFP-expressing MDCKII cells and RFP-expressing MDCKI cells were seeded at a 1:4 ratio 2 d before time-lapse imaging. Mouse intestinal organoids were prepared from female C57BL/6N mice (SLC) and maintained as described in (Mahe et al., 2013).

Drosophila genetics and maintenance

Flies were grown at 25 °C and fed with standard fly food. Females were isolated from males 1–3 d after eclosion and used for analysis. For experiments using the GeneSwitch system (Osterwalder et al., 2001) flies were transferred to a vial with food containing 73 μg/mL Mifepristone (Sigma Aldrich, M8046) 5 d after eclosion. Adult flies were transferred to new vials containing Mifepristone every 2 days. Myo1A-Gal4 (112-001) and Esg-GFP (114-268) were obtained from Kyoto Stock Center (DGRC). UAS-*Arf51F* RNAi (51417), UAS-*Arf79F* RNAi (66174), UAS-*Xk* (CG32579) RNAi (57784), RNAi isogenic control (36303, 36304), UAS-Arf51F:GFP (65867), Eip71CD-Gal4 (6871), hs-FLPG5 (55817), act < cd2 < Gal4, UAS-RFP (30558), and UAS-mCD8:mRFP (27398) were obtained from Bloomington Drosophila Stock Center (BDSC). UAS-*Xk* (CG32579) RNAi (110645), RNAi isogenic control (60100), and UAS-Dicer2 (60007) were obtained from Vienna Drosophila Resource Center (VDRC). Lgl:GFP was provided by Dr. Y. Hong; Pswitch CSG5966, Dr. E. Piddini; Tsh-Gal4, Dr. T. Tabata; DE-

Cad:GFP, Dr. Y. Oda; Sqh:mKate2, Dr. Y. Bellaïche; UAS-AnnexinV:GFP and UAS-AnnexinV (mutant):GFP, Dr. C. Han; act < y+ < LexA, LexAop-CD8:GFP, Dr. L. LeGoff. For clonal analysis, 13–19 d after eclosion (grown at 18 °C), flies were heated at 37 °C for 15 min. After 7 d (grown at 25 °C), their midguts were dissected and observed using laser confocal microscope.

The genotypes of the *Drosophila* lines used in Figures and Supplemental Figures

Figure	Genetype	
3B, D	Lgl:GFP/+	Pupa
3C	Eip71CD-Gal4, Lgl:GFP/UAS-mCD8:mRFP	Pupa
3E	Esg-Gal4/UAS-AnnexinV: GFP or UAS-AnnexinV (mutant):GFP	Pupa
3F, G	Esg-Gal4, Lgl:GFP/UAS-AnnexinV: GFP or UAS-AnnexinV (mutant):GFP	Pupa
3H	Tsh-Gal4/UAS-AnnexinV: GFP or UAS-AnnexinV (mutant):GFP	Adult (abdomen)
3I, J	Tsh-Gal4, Lgl:GFP/UAS-Xk (CG32579) RNAi or +	Pupa
3K	Tsh-Gal4, DE-Cad:GFP/UAS-Xk (CG32579) RNAi or +	Pupa
4B	Sqh:mKate2, Lgl:GFP	Pupa
4E	Tsh-Gal4, Sqh:mKate2/UAS-Arf51F:GFP	Pupa
4F, G, H	Tsh-Gal4, Lgl:GFP/UAS-*Arf51F* RNAi or +	Pupa
S3B	hs-FLPG5; act < cd2 < Gal4, UAS-RFP/act < y+ < LexA, LexAop-CD8:GFP	Adult (midgut)
S3C	UAS-Dicer2; Pswitch CSG5966/+	Adult (midgut)
S4A, C	UAS-Dicer2; Pswitch CSG5966/UAS-Xk (CG32579) RNAi (BDSC) or +	Adult (midgut)
S4B	UAS-Dicer2; Pswitch CSG5966/UAS-Xk (CG32579) RNAi (VDRC) or UAS-Xk (CG32579) RNAi (BDSC) or +	Adult (midgut)
S4D, E, F	UAS-Dicer2; Pswitch CSG5966/UAS-*Arf79F* RNAi or +	Adult (midgut)

Time-lapse imaging

Cells were seeded on a tissue culture-treated glass-bottom dish (CELLVIEW™ CELL CULTURE DISH, Greiner Bio-One, 627870). After 2 or 3 d (1 d after the cells reached a confluent state), time-lapse images were acquired. The standard culture medium was replaced with FluoroBrite™ DMEM (Thermo Fisher, A1896701) containing 5% or 10% FBS, antibiotics, and GlutaMax™ Supplement (Thermo Fisher, 35050061) 1 h before imaging. For the overexpression of MFG-E8 (D89E), the medium change was done 6 h before imaging to accumulate the secreted MFG-E8 (D89E) protein in the medium. Most of time-lapse images were acquired using a laser confocal microscope (TCS SP8, Leica or FV3000, Olympus) equipped with a 20× or 63× oil-immersion objective, a time-lapse module, and a multi-position

module in a chamber (Tokai Hit) containing 5% CO_2 and at 37 °C. A hybrid detector (Leica) was used for the detection in TSC SP8. Las X software (Leica) or was used for analysis of confocal images and movie file preparation. All images and movies used in the report were prepared from confocal images at a single z-position unless otherwise stated.

RNA-seq analysis

Total RNA was isolated from EpH4 cells or adult *Drosophila* midguts using an RNAeasy micro kit (Qiagen) with DNaseI treatment according to the manufacturer's instructions. For the *Drosophila* experiment, the posterior part of the midguts of 15 adult flies were homogenized using a syringe with a 26G needle (Terumo) in the RLT solution provided with the kit. After RNA integrity was confirmed using an Agilent RNA 6000 Nano Chip (Agilent Technologies), total RNA samples were used for RNA-seq library preparation using an Illumina TruSeq Stranded mRNA LT sample kit according to the manufacturer's instructions (Illumina). The pooled libraries were sequenced on an Illumina NextSeq500 sequencing platform, and approximately 20 million raw reads for each sample were obtained by single-end sequencing of 76 bp length. The obtained reads were mapped to the reference genome (GRCm38 for EpH4 cells and BDGP assembly release 6 for adult *Drosophila* midgut) using TopHat2 (Kim et al., 2013) and the FPKM (fragments per kilobase of exon per million reads mapped reads) values were defined using cuffdiff (Trapnell et al., 2012).

Analysis of *Drosophila* pupal epidermis

Pupae were collected 16–18 h after pupal formation and placed on double-sided tapes attached to glass slides. The pupal case was removed, and Halocarbon oil 700 (Sigma Aldrich, H8898) was

added to the dorsal abdomen, which was then covered with cover glass. Time-lapse imaging was performed using laser confocal microscope with multi-positioning and adaptive focus control modes.

Quantitative and statistical analysis

Quantification was performed using the basic measurement tool in Fiji/ImageJ. To quantify cell protrusion from the cell layer, sequential confocal images were analyzed, and the length between the apex of extruding cells and the surface of the neighboring cell layer was calculated. To quantify the width of LEC region, maximum projection images of z-stacks of up to 200 μm were analyzed. To quantify the progress of extrusion of LECs, the length from the apical surface of cell layer to a section in which the width of the extruding cell is at the maximum was calculated. Two-tailed Welch's *t*-tests were used to determine *P*-values. *P*-values < 0.05 were considered significant. Survival curves were analyzed using the log-rank test with BellCurve for Excel (Social Survey Research Information). In box-and-whisker plots outliers are always plotted as crosses.

Immunostaining and other staining methods

Drosophila midguts were dissected in PBS, fixed with 4% paraformaldehyde in phosphate buffer (Wako) for 1 h at 25 °C, and post-fixed with methanol for 30 min at −30 °C. After permeabilization with 0.1% (v/v) Triton X-100 in PBS and blocking with Blocking One (Nakarai Tesque, 03953-66), the midguts were incubated with mouse anti-discs large monoclonal antibody (4F3) (1:100, Developmental Studies Hybridoma Bank) and subsequently with Alexa Fluor 546 conjugated goat anti-mouse IgG (1:1000, Life Technology, A11003). Counterstaining

was performed with 1 μg/mL of DAPI (Wako, 340-07971) and Phalloidin-TRITC (1:2000 Sigma Aldrich, P1951).

Cultured cells were seeded in a chamber slide (Matsunami) 2 or 3 d before the staining experiments. Cells were fixed with 1% paraformaldehyde in PBS for 20 min at 25 °C. After permeabilization with 0.1% (v/v) Triton X-100 in PBS and blocking with Blocking One (Nakarai Tesque), samples were incubated with rabbit anti-cleaved caspase3 monoclonal antibody (Asp175) (1:300, Cell Signaling Technology, 9661) and then Goat anti-Rabbit IgG (H+L) Cross-Absorbed Secondary Antibody, Alexa Fluor 488 (1:1200, Life Technology, A11008). Counterstaining with 0.5 μg/mL of DAPI and Phalloidin-TRITC (1:2000) was performed.

For Annexin V staining of cultured cells, Annexin V Alexa Fluor™ 555-conjugate (1:20, Molecular Probes, A35108) was used for staining with 1 μg/mL of Hoechst33342 (Wako, 346-07951) according to the manufacturer's instruction. Before staining, the cell layer was scratched at some points with a microtip to allow Annexin V to access the basolateral parts of cells. Images were captured within 30 min after the completion of staining.

To visualize the cell membrane, 2.5 μg/mL of CellMask™ Deep Red Plasma membrane Stain (Thermo Fisher, C10046) was added 1 hour before the acquisition of time-lapse images. For lysosome staining, 150 nM of LysoTracker™ Red DND-99 (Thermo Fisher, L7528) was added 1 h before the acquisition of time-lapse images.

Mathematical model and numerical analysis

Cellular Potts model (CPM)

We modeled the dynamics of cells and EVs on the vertical section of the cell monolayer using a two-dimensional CPM, which is widely used to represent the complex interactions of different

objects at multiple scales (Boas and Merks, 2014; Glazier and Graner, 1993; Hino et al., 2020; Hirashima et al., 2017; Merks and Glazier, 2005). Individual forms of cells and EVs are represented as a collection of squared lattices, each of which is labeled with a lattice index (σ) and a type index (τ), which can represent extruding cells, non-extruding remaining cells, EVs, or the medium, that is, $\tau \in \{c^*, c, v, m\}$. Owing to its straightforward expression, CPM can handle the complex shapes of different types of objects.

An arrangement of lattices specifies the value of the total energy in the system (H) according to the given functions. The total energy in the model consists of the minimal factors necessary to capture the dynamics of cells and EVs and interactions between those objects at the section of interest, such as interfacial adhesion, size maintenance, and active force, as follows:

$$H = H_{adhesion} + H_{size} + H_{active}. \quad (1)$$

The first term of Eq. (1) is the interfacial adhesion energy between different objects, such as cell-cell, cell-EV, and cell-medium, formulated as:

$$H_{adhesion} = \sum_{\boldsymbol{r},\boldsymbol{s}} J_{\tau(\sigma_{\boldsymbol{r}})\tau(\sigma_{\boldsymbol{s}})}\left(1 - \delta_{\sigma_{\boldsymbol{r}}\sigma_{\boldsymbol{s}}}\right), \quad (2)$$

, where $\boldsymbol{r}$ and $\boldsymbol{s}$ represent the positions of the lattice sites, J is the interfacial energy between the different objects, and δ is the Kronecker delta. In the simulations, the adhesion energies between the same cell types were set to $J_{c^*c^*} = J_{cc} = 2$, and those between the cells and medium were set to $J_{c^*m} = J_{cm} = 10$, based on a previous study (Glazier and Graner, 1993). Thus, the adhesion energy between extruding cells and non-extruding cells, J_{c^*c}, controls the decrease in

adhesion, defined as $\Delta = J_{c^*c} - J_{cc}$. Note that $c^*, c,$ and, m denote the extruding cells, non-extruding cells, and medium, respectively.

The second term of Eq. (1) represents the size constraint of the cells and EVs in a quadratic form:

$$H_{size} = \sum_{\sigma,\tau=\{c^*,c\}} (S_\sigma - S^{cell})^2 + \sum_{\sigma,\tau=\{v\}} (S_\sigma - S_\sigma^{EV})^2 , \quad (3)$$

, where S_σ is the current cell size, S^{cell} is the target cell size, and S_σ^{EV} is the target EV size. $S^{cell} = 200\ [\mu m^2]$ was determined based on the experiments, and S_σ^{EV} is a variable described below.

The third term of Eq. (1) includes lamellipodia cell protrusions as a result of active cellular force as follows:

$$H_{active} = -\lambda_c A_{\sigma,c}, \quad (4)$$

, where λ_c is the weight parameter of the lamellipodia protrusions, and $A_{\sigma,c}$ is the basal area of non-extruding cells specified in the apico-basal range between the surface of the substrate and one-tenth of the initial cell height, defined as the height of the lamellar zone *H* (Figure S5B). Note that this energy term is only effective for non-extruding cells. Thus, the basal side of the extruding cell was occupied by the lamellipodia of the neighboring non-extruding cells. As the lamellipodia extrusions affected cell extrusion less, we arbitrarily set $\lambda_c = 100$ in the simulations.

Briefly, the system transition in CPM occurs stochastically using a lattice-based Monte Carlo method (Glazier and Graner, 1993; Hirashima et al., 2017; Merks and Glazier, 2005). That is, the labeled value of a randomly chosen lattice site, $\sigma_{\boldsymbol{r}}$, is replaced by a different labeled value of an adjacent lattice site, $\sigma_{\boldsymbol{s}}$, which is randomly chosen. This transition can be realized by evaluating the change in the energy ΔH associated with its replacement. The replacement occurs stochastically according to the Boltzmann acceptance function $\exp(-\Delta H/T)$ when $\Delta H > 0$, but it occurs deterministically when $\Delta H \leq 0$. We set the controlling parameter of the fluctuation to $T = 3$. Repeating the trials for lattice replacement, the systems gradually transitioned to a lower-energy state. We regarded the total number of pixel domains in the simulations as a unit of the simulation step, Monte Carlo step (mcs), and 100 mcs to 1 min.

EV dynamics

EV formation was modelled as a discrete event in the simulations. Single EVs were sequentially produced at regular time intervals, labelled as τ by replacing the peripheral lattices of the extruding cell within a spatial range. For the simulations other than Figure 6D, the EV zone, where the EVs were potentially generated, was specified between the upper limit (the center of mass of extruding cells) and the lower limit (the parameter *L*) (Figure S5B). To investigate the impact of the EV formation region in Figure 6D, the spatial range of EV formation was specified based on the angle at the upper limit for different regions, including the 1) basal, 2) lateral, and 3) apical sides. Within the specified range, a source lattice of EV formation was randomly selected if the space was available, and the EV region was then formed around the source lattice. The EV that decayed once formed as:

$$\dot{S}_{\sigma}^{EV} = -\gamma S_{\sigma}^{EV}, \quad (5)$$

, where γ is the decay rate of the EV. Note that the decay effect encompasses various biological processes, such as degradation, random movement, and engulfment by non-extruding cells.

Simulation settings

Simulations were conducted in a lattice domain of 420 × 80 pixels. The virtual cell monolayer, which was placed on the bottom edge of the domain, was composed of seven cells arranged horizontally. At initial conditions, the width and height of each cell were set to 20 μm (60 pixels) and 10 μm (30 pixels), respectively, according to the observations. We assumed an undeformable substrate at the bottom side of the simulation domain and set a periodic boundary along the horizontal axis and a fixed boundary along the vertical axis. Regarding the sequence of events, one cell at the center of the cell monolayer was selected as the extruding cell at 0 mcs, and EV formation in the extruding cells began at 50 mcs. The calculation ended at 1050 mcs.

Supplementary Figures and Table:

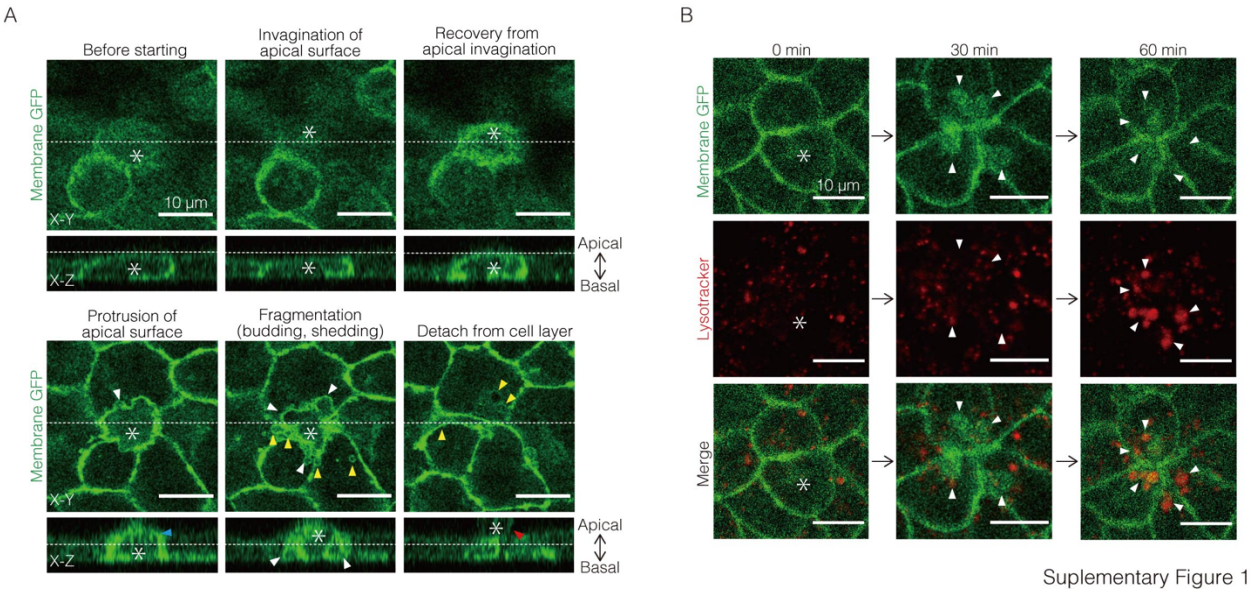

Suplementary Figure 1

5

Figure S1. Cell extrusion processes

(A) The processes during cell extrusion in MDCKII cells. Representative images for each process in palmitoylated GFP (membrane GFP, green)-expressing extruding MDCKII cells. Corresponds to Figure 1C. Fragmentation is defined as budding and shedding of vesicles formed in extruding cells. Asterisks indicate an extruding cell. White arrowheads indicate budding in fragmentation; yellow arrowheads, engulfed fragments after shedding; blue arrowhead, protrusion of extruding cell; and a red arrowhead, cell detachment from the cell layer. Dashed lines correspond to the position from another angle (x-y or x-z images).

(B) Lysosomal transport of engulfed vesicles derived from the fragmentation of extruding cells. Lysotracker staining (red) in palmitoylated GFP (membrane GFP, green)-expressing MDCKII cells. The engulfed vesicles in the neighboring cells were positive for the lysotracker signal (32/36 extrusion events) 30–60 min after incorporation. Asterisks indicate an extruding cell, whereas arrowheads indicate engulfed fragments.

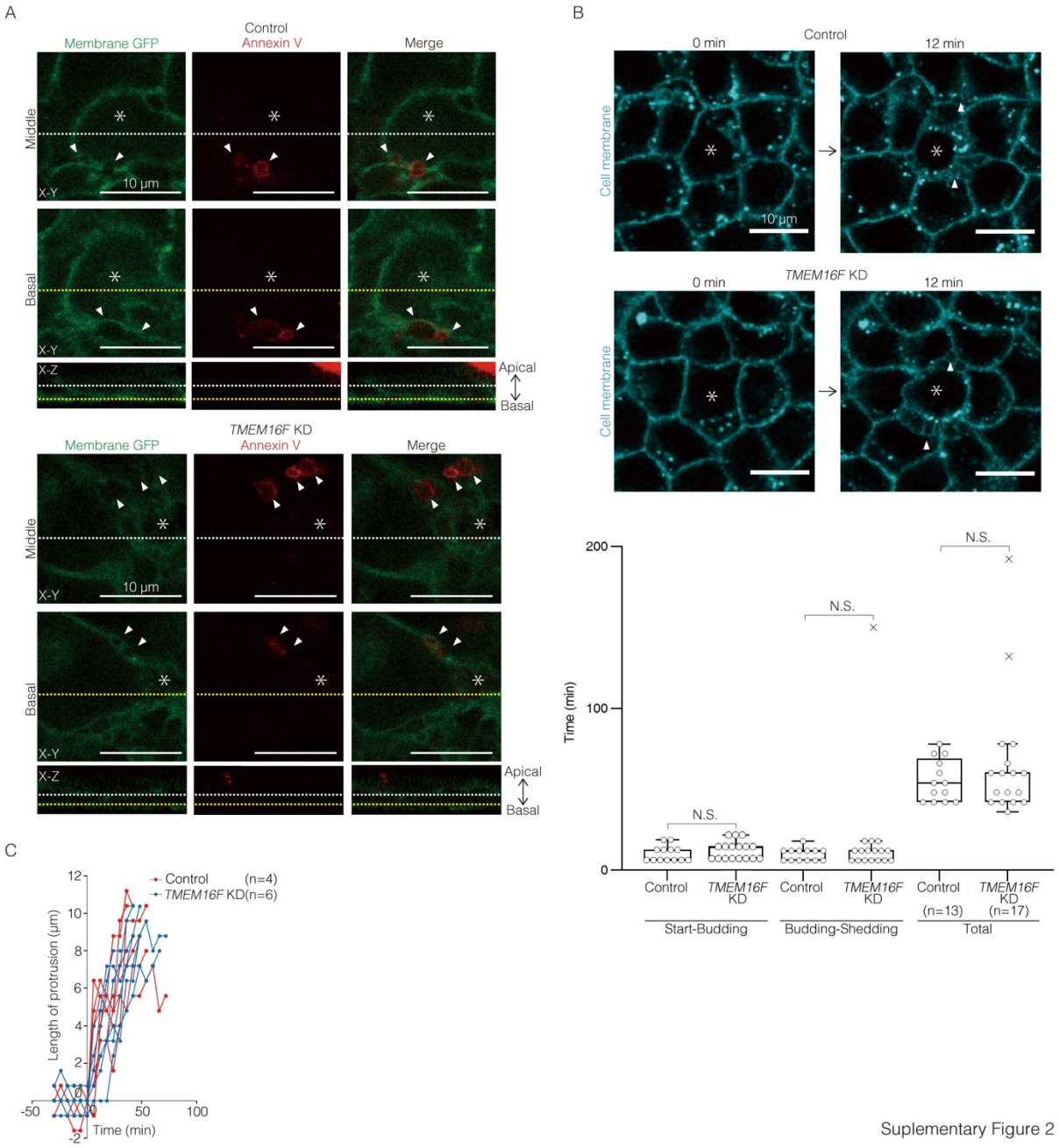

Suplementary Figure 2

Figure S2. TMEM16F (Ano6) is not required for the fragmentation of extruding cells and cell extrusion in EpH4 cells

(A) Representative images of Annexin V (red)-stained control (scrambled siRNA) and *TMEM16F*-siRNA palmitoylated GFP (membrane GFP, green)-expressing EpH4 cells. Asterisks indicate extruding cells. Arrowheads indicate cell fragmentation. White and yellow dashed lines correspond to the position from another angle at the middle part and basal part in x-z axis, respectively.

(B) Representative images and quantification of time for indicated processes in the control and *TMEM16F*-siRNA extruding EpH4 cells stained with CellMask (cyan). Asterisks indicate extruding cells, whereas arrowheads indicate fragments in the intercellular space. Crosses in a box-and-whisker plot indicate outliers.

(C) Quantification of the apical protrusion of extruding cells in the control (red) and *TMEM16F*-siRNA (blue) EpH4 cells. Time 0 is defined as the start of cell extrusion (cell deformation).

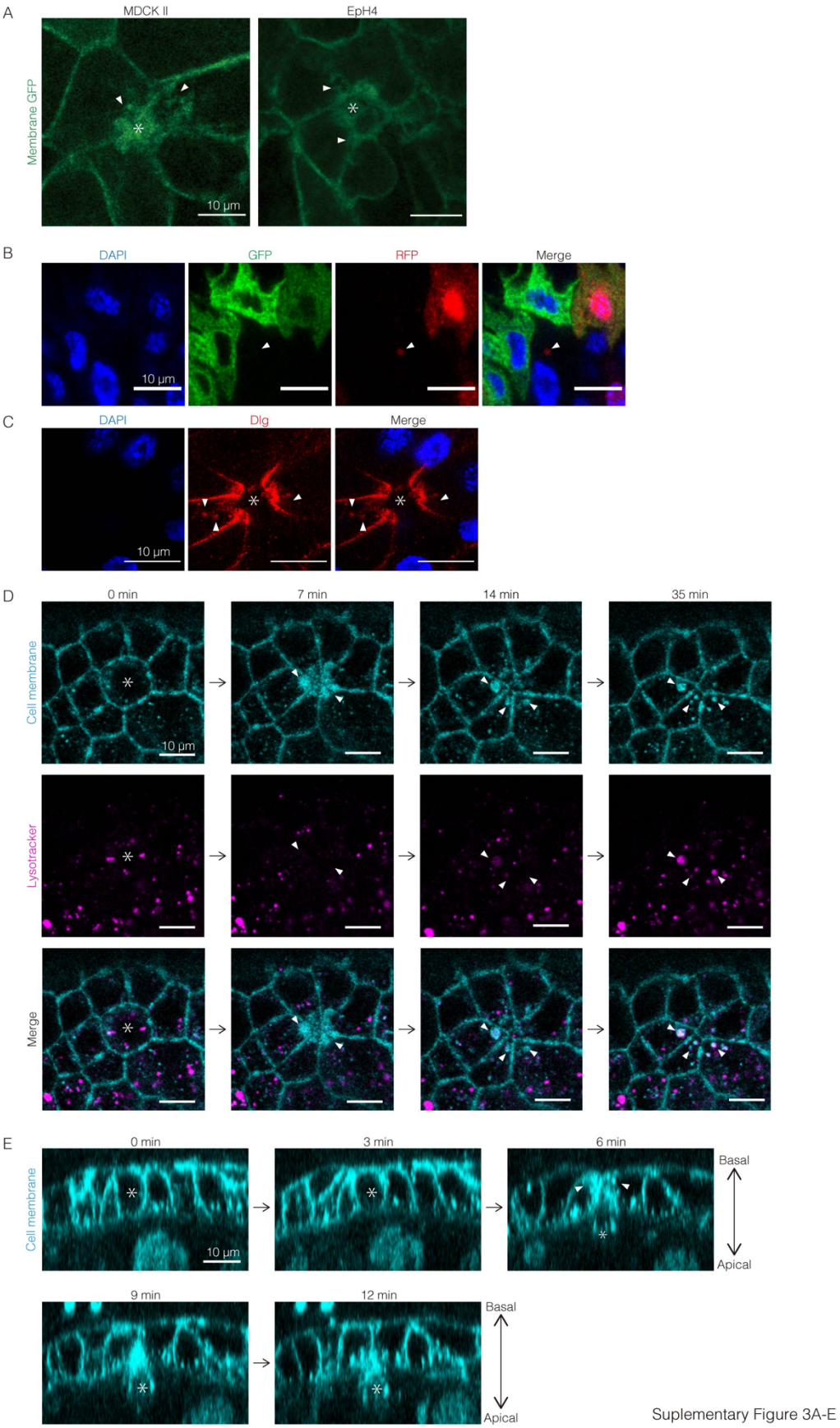

Suplementary Figure 3A-E

F

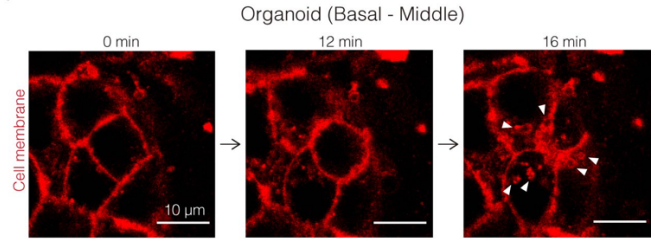

G

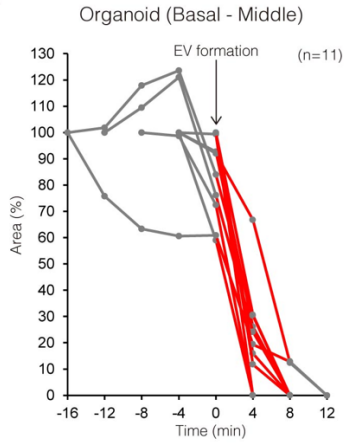

H

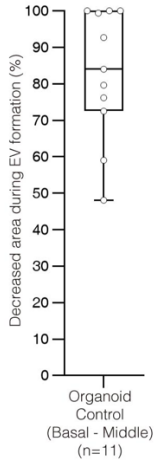

Suplementary Figure 3F-H

Figure S3. Universality of fragmentation in extruding cell

(A) Cell fragmentation in UV irradiation-induced cell extrusion. Palmitoylated GFP (membrane GFP, green)-expressing MDCKII and EpH4 cells were irradiated by 180 and 150 mJ of UV, respectively, and images were acquired 17 and 24 h after irradiation. Asterisks indicate extruding cells, whereas arrowheads indicate fragments in the intercellular space or those engulfed by neighboring cells.

(B and C) Fragmentation and engulfment in adult *Drosophila* midgut epithelium. (B) Representative images of cell mosaic in the midgut epithelium, wherein each epithelial cell randomly expresses GFP (green) and/or RFP (red) or neither, stained with DAPI (blue). RFP-positive vesicles (arrowheads) were observed in the fluorescent non-expressing cell. (C) Immunostaining for Dlg (red) with DAPI (blue) in the midgut epithelium. Engulfed fragments (arrowheads) in the neighboring cells adjacent to an extruding cell (asterisks) were observed.

(D and E) Fragmentation at the basal half of the extruding cells in mouse intestinal organoid. (D) Representative x-y images of an extruding cell in mouse intestinal organoid stained with CellMask (cyan) and lysotracker (magenta). Asterisks indicate extruding cells, whereas arrowheads indicate fragments engulfed by neighboring cells.

(E) Representative transverse optical section of a cell, which extrude to the apical direction, in the organoid stained with CellMask (cyan). Asterisks indicate extruding cells, whereas arrowheads indicate fragmentation at the basal part of extruding cell.

(F) Representative images of an extruding cell in mouse intestinal organoid stained with CellMask at the x-y plane where EV formation most frequently occurs (Basal-Middle: basal half but closed to the border of apical and basal half). Arrowheads indicate shed and engulphed EVs.

(G) Quantified evolution of cell area at the Basal-Middle x-y plane (shown in A) in extruding

mouse intestinal organoid cells. 100% is defined as the area at the start of cell extrusion. Red lines indicate the period of EV shedding. Time 0 is defined as the start of EV shedding (EV formation).

(H) Ratio of decreased area during EV shedding (i.e., EV formation) at the Basal-Middle x-y plane in extruding mouse intestinal organoid cells.

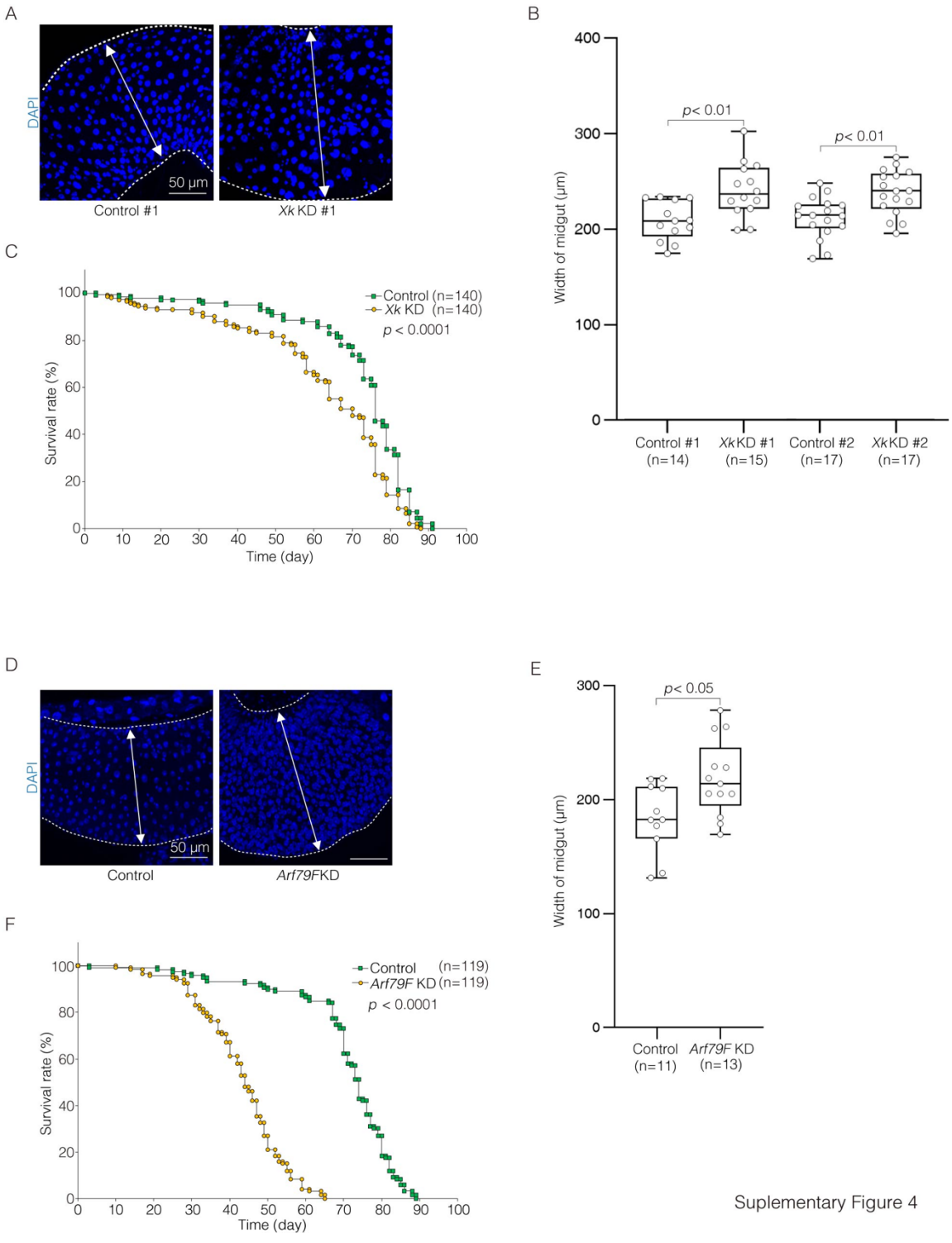

Suplementary Figure 4

Figure S4. Impaired homeostasis in EV related gene-knocked down *Drosophila*

Xk- (A–C) or *Arf79F*- (D–F) knockdown in adult *Drosophila* midgut. Gene knockdown by RNAi was induced in the adult stage in a midgut enterocyte-specific manner using the GeneSwitch system.

(A and D) Representative maximum projection images of the isogenic control and the RNAi midgut (region 4 (Buchon et al., 2013)) stained with DAPI (blue). Dashed lines indicate each midgut.

(B and E) Width of region 4 in the isogenic control and the RNAi midguts measured by the length as indicated by double-sided arrows in (A and D).

(C and F) Survival curves of the isogenic control (green) and the RNAi (yellow) *Drosophila. P*-value is determined using the log-rank test.

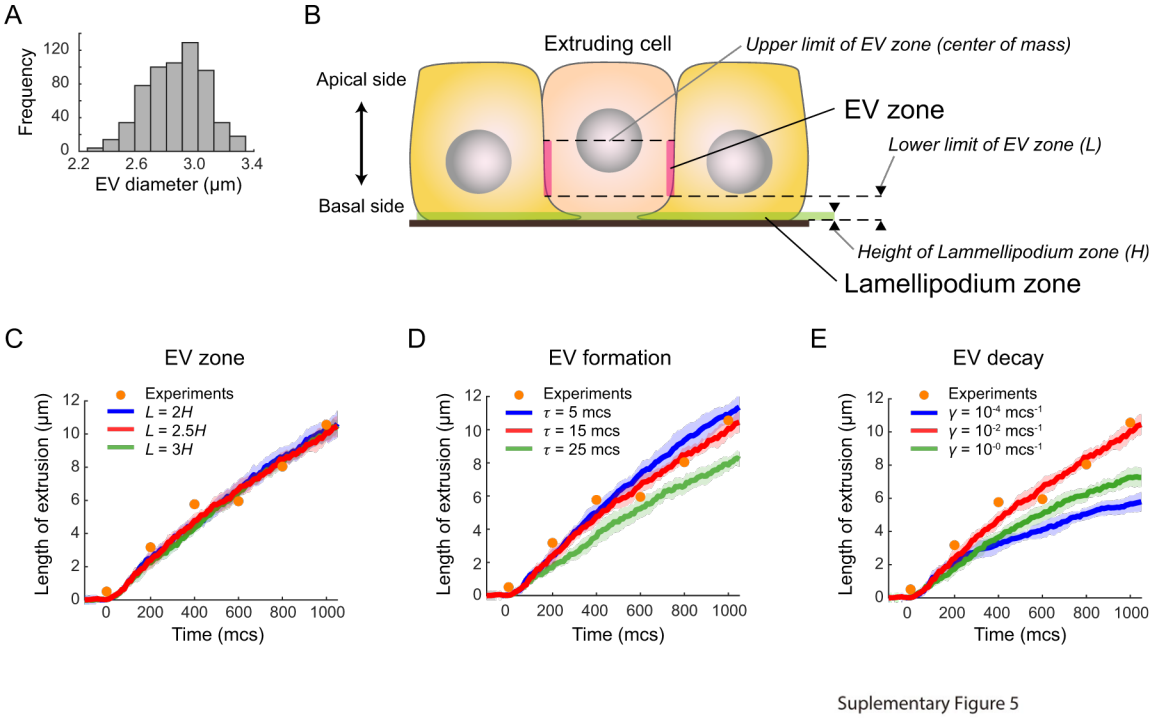

Suplementary Figure 5

Figure S5. Parameter dependency of cell extrusion dynamics

(A) Histogram of EV diameter at its formation. The mean value is 2.9, and the standard deviation (s.d.) is 0.2; n=612.

(B) The schematic model parameters. The upper limit of EV zone was defined as the center of mass of the extruding cell. The lower limit of EV zone L was determined based on the height of lamellipodium zone H.

(C–E) Dependency of the cell extrusion dynamics on parameters: the lower limit of EV zone L (C), time interval of EV formation τ (D), and EV decay rate γ (E). The standard parameters values were shown in red. There were no significant changes within the parameter range of EV zone, and the standard value of L was determined by eyes. Mean ± s.d. (n=10). Orange dots represent the mean values of experimental data (n=5).

.

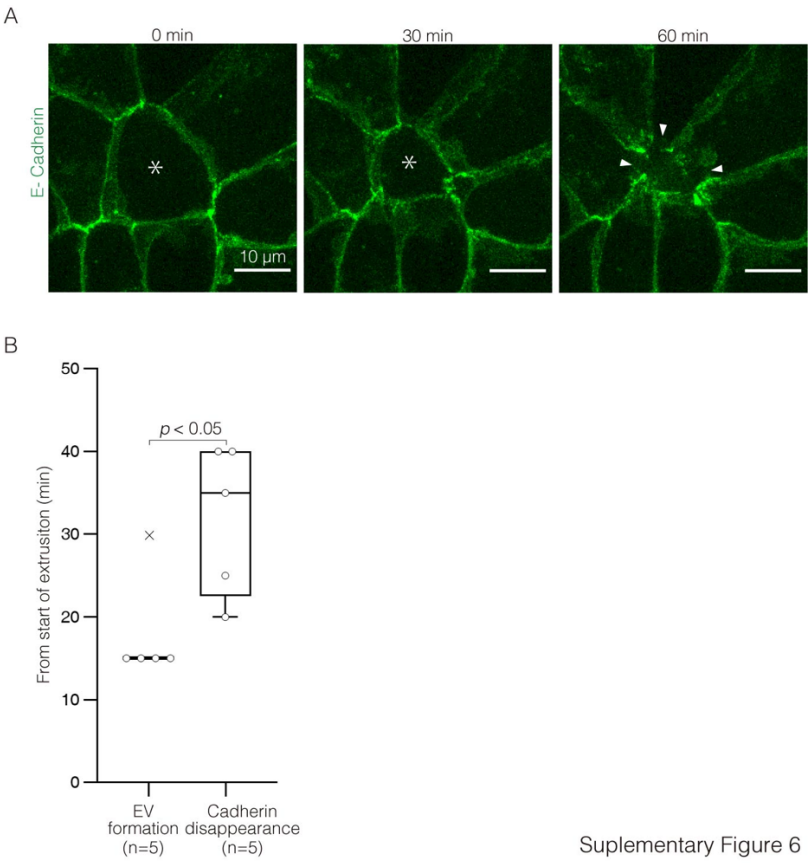

Suplementary Figure 6

Figure S6. EV formation occurs prior to the disappearance of adherens junction in EpH4 cell

(A) Representative images of disappearance of adherens junctions (arrowheads) of E-Cadherin:GFP-expressing extruding (asterisk) EpH4 cell.

(B) Quantification of the timing of EV formation and the disappearance of adherens junction in extruding E-Cadherin:GFP-expressing EpH4. Crosses in a box-and-whisker plot indicate outliers.

Table S1. Gene expression from RNAseq analysis in EpH4 cell and *Drosophila* adult midgut

Fragments per kilobase of exon per million reads mapped (FKPM) of some Arf family genes, TMEM16 family genes, and Xkr family genes in RNAseq analysis of EpH4 cell and *Drosophila* midgut is shown. The number of biological replicates was three.

EpH4 cell

		FPKM				
gene name	gene ID	Replicate 1	Replicate 2	Replicate 3	Average	SD
Arf1	ENSMUSG00000048076	291.043	394.692	327.569	337.768	52.571794
Arf6	ENSMUSG00000044147	36.2654	35.495	33.4041	35.0548333	1.4805639
Ano3	ENSMUSG00000074968	0.0159882	0	0	0.0053294	0.0092308
Ano4	ENSMUSG00000035189	0	0.015948	0.955046	0.32366467	0.5468504
Ano6	ENSMUSG00000064210	25.2188	34.5515	30.4293	30.0665333	4.6769137
Ano7	ENSMUSG00000034107	0	0	0	0	0
Ano9	ENSMUSG00000054662	2.68279	1.96306	2.8719	2.50591667	0.4795421
Xkr4	ENSMUSG00000051951	0	0	0	0	0
Xkr8	ENSMUSG00000037752	0.897262	2.19177	0.900079	1.32970367	0.7465727
Xkr9	ENSMUSG00000067813	0	0	0	0	0

Drosophila midgut

		FPKM				
gene name	gene ID	Replicate 1	Replicate 2	Replicate 3	Average	SD
arf51f (arf6)	FBgn0013750	51.3448	42.221	48.1021	47.2226333	4.6250435
arf79f (arf1)	FBgn0010348	498.962	418.416	455.613	457.663667	40.312138
xk (CG32579)	FBgn0052579	9.36984	10.4461	9.0385	9.61814667	0.7359189

Captions for Supplementary Movies:

Movie S1

Corresponds to Figure 1A. Cell extrusion of a palmitoylated GFP (green)-expressing MDCKII cell. A time-lapse image with a single z-position at 63× magnification. Scale bar, 10 μm

Movie S2

Corresponds to Figure 1D. Co-culture of palmitoylated GFP- and RFP-expressing MDCKII cells. Cell extrusion of a RFP (red)-expressing cell adjacent to palmitoylated GFP (green)-expressing cells. A time-lapse image with a single z-position at 63× magnification. Scale bar, 10 μm

Movie S3

(A) Corresponds to Figure 2E. Cell extrusion of a palmitoylated GFP (green)-expressing EpH4 cells. A time-lapse image with a single z-position at 63x magnification. Scale bar, 10 μm

(B) Corresponds to Figure 2F. Cell extrusion of a MFG-E8 D89E mutant protein- and palmitoylated GFP (green)-expressing EpH4 cell. A projected (3 confocal images, 0.75 μm interval each) time-lapse image at 63x. Scale bar, 10 mm

Movie S4

Corresponds to Figure 3B. Cell extrusion of a Lgl:GFP (green)-expressing LEC in the basal direction. A time-lapse image at 63x magnification. Scale bar, 10 μm.

Movie S5

Corresponds to Figure 3E. Cell extrusion of an AnnexinV:GFP (green)-expressing LEC (dotted line). A projected (3 confocal images in apical site, 1 μm interval each) time-lapse image at 63x magnification. Scale bar, 10 μm.

Movie S6

Corresponds to Fig. S3D. Cell extrusion of a cell in mouse intestinal organoid stained with CellMask (cyan) and lysotracker (magenta). A time-lapse image with a single z-position at 63× magnification. Scale bar, 10 μm.

Movie S7

Corresponds to Figure 4J. Apoptotic FDC/P1 cells without (A) or with (B) PLD1 inhibitor. A time-lapse image with a single z-position at 20× magnification. Scale bar, 10 μm.

Movie S8

Corresponds to Figure 5A. Most basal plane (A) and Basal-Middle (basal half but closed to the border of apical and basal half) plane (B) of a palmitoylated GFP (green)-expressing MDCKII cells. A time-lapse image with a single z-position at 63x magnification. Scale bar, 10 μm

Movie S9

Corresponds to Figure 6B. Model simulations in the presence (upper) and the absence (lower) of EVs. Scale bar, 10 μm.

Movie S10

Corresponds to Figure 6F. Model simulations in different values of the EV turnover rate and the cell-cell adhesion: slow EV turnover (upper), fast EV turnover (middle), and no decrease of adhesion (lower).

References

Boas, S.E.M., and Merks, R.M.H. (2014). Synergy of cell–cell repulsion and vacuolation in a computational model of lumen formation. J. R. Soc. Interface *11*, 20131049.

Buchon, N., Osman, D., David, F.P.A., Yu Fang, H., Boquete, J.-P., Deplancke, B., and Lemaitre, B. (2013). Morphological and Molecular Characterization of Adult Midgut Compartmentalization in Drosophila. Cell Rep. *3*, 1725–1738.

Glazier, J.A., and Graner, F. (1993). Simulation of the differential adhesion driven rearrangement of biological cells. Phys. Rev. E *47*, 2128–2154.

Hanayama, R., Tanaka, M., Miwa, K., Shinohara, A., Iwamatsu, A., and Nagata, S. (2002). Identification of a factor that links apoptotic cells to phagocytes. Nature *417*, 182–187.

Hino, N., Rossetti, L., Marín-Llauradó, A., Aoki, K., Trepat, X., Matsuda, M., and Hirashima, T. (2020). ERK-Mediated Mechanochemical Waves Direct Collective Cell Polarization. Dev. Cell *53*, 646-660.e8.

Hirashima, T., Rens, E.G., and Merks, R.M.H. (2017). Cellular Potts modeling of complex multicellular behaviors in tissue morphogenesis. Dev. Growth Differ. *59*, 329–339.

Kim, D., Pertea, G., Trapnell, C., Pimentel, H., Kelley, R., and Salzberg, S.L. (2013). TopHat2: accurate alignment of transcriptomes in the presence of insertions, deletions and gene fusions. Genome Biol. *14*, R36.

Mahe, M.M., Aihara, E., Schumacher, M.A., Zavros, Y., Montrose, M.H., Helmrath, M.A., Sato, T., and Shroyer, N.F. (2013). Establishment of Gastrointestinal Epithelial Organoids. Curr. Protoc. Mouse Biol. *3*, 217–240.

Masuda, S., Oda, Y., Sasaki, H., Ikenouchi, J., Higashi, T., Akashi, M., Nishi, E., and Furuse, M. (2011). LSR defines cell corners for tricellular tight junction formation in epithelial cells. J. Cell Sci. *124*, 548–555.

Merks, R.M.H., and Glazier, J.A. (2005). A cell-centered approach to developmental biology. Phys. Stat. Mech. Its Appl. *352*, 113–130.

Osterwalder, T., Yoon, K.S., White, B.H., and Keshishian, H. (2001). A conditional tissue-specific transgene expression system using inducible GAL4. Proc. Natl. Acad. Sci. *98*, 12596–12601.

Trapnell, C., Roberts, A., Goff, L., Pertea, G., Kim, D., Kelley, D.R., Pimentel, H., Salzberg, S.L., Rinn, J.L., and Pachter, L. (2012). Differential gene and transcript expression analysis of RNA-seq experiments with TopHat and Cufflinks. Nat. Protoc. *7*, 562–578.